Tissue-specific programming of memory CD8 T cell subsets impacts protection against lethal respiratory virus infection

Georges Abboud, Pritesh Desai, Farhad Dastmalchi, Jessica Stanfield, Vikas Tahiliani, Tarun E. Hutchinson, and Shahram Salek-Ardakani

Department of Pathology, Immunology, and Laboratory Medicine, University of Florida, Gainesville, FL 32611

How tissue-specific anatomical distribution and phenotypic specialization are linked to protective efficacy of memory T cells against reinfection is unclear. Here, we show that lung environmental cues program recently recruited central-like memory cells with migratory potentials for their tissue-specific functions during lethal respiratory virus infection. After entering the lung, some central-like cells retain their original CD27^{hi}CXCR3^{hi} phenotype, enabling them to localize near the infected bronchiolar epithelium and airway lumen to function as the first line of defense against pathogen encounter. Others, in response to local cytokine triggers, undergo a secondary program of differentiation that leads to the loss of CXCR3, migration arrest, and clustering within peribronchoarterial areas and in interalveolar septa. Here, the immune system adapts its response to prevent systemic viral dissemination and mortality. These results reveal the striking and unexpected spatial organization of central- versus effector-like memory cells within the lung and how cooperation between these two subsets contributes to host defense.

The Journal of Experimental Medicine

INTRODUCTION

Memory CD8 T cells have traditionally been classified as either central memory cells (CCR7^{hi}CD62L^{hi}; Tcm) that recirculate through the blood and secondary lymphoid organs, or effector memory cells (CCR7^{lo}CD62L^{lo}; Tem) that transit through blood and peripheral tissues, such as the lung (Sallusto et al., 1999; Masopust et al., 2001; Jameson and Masopust, 2009; Sathaliyawala et al., 2013; Thome et al., 2014). Recent studies performed in several experimental systems suggest that Tcm and Tem can be further separated into two major subsets based on their expression of CD27: CD27^{hi} central-like (Tcm-l) and CD27^{lo} effector-like (Tem-l) cells (Hikono et al., 2007; Olson et al., 2013). In the spleen, CD27^{hi} cells predominantly reside in the T cell–rich areas of periarteriolar lymphocyte sheath (PALS) and exhibit optimal recall proliferative and self-renewal potential (Hikono et al., 2007; Jung et al., 2010). In contrast, CD27^{lo} cells fail to undergo significant recall proliferation, but efficiently home to the red pulp and the marginal zone surrounding the white pulp (Hikono et al., 2007; Olson et al., 2013). The origins of these memory T cell subsets and how they relate to each other are still being elucidated. One possibility is that long-lived CD27^{lo} Tem-l memory cells participate directly in the initiation of protective recall responses by rapidly producing cytolytic proteins at sites of pathogen entry, whereas activation of CD27^{hi} Tcm-l memory cells is required for the generation of new rounds of effector memory T cells, and thus, may contribute to the maintenance and/or amplification of the overall response. Consistent with this idea, a recent study by Olson et al. (2013) demonstrated that despite their poor proliferative potential, CD27^{lo} cells in the spleen provide superior protection against systemic (i.v.) infection with either *Listeria monocytogenes* or vaccinia virus (VACV), supporting the concept that to protect against rapidly replicating blood-borne pathogens, high-numbers of CD27^{lo} Tem-l cells need to be present at the site of pathogen entry.

Pathogen-specific CD27^{lo} memory cells also persist in mucosal tissues, such as the lung (Hikono et al., 2007). However, there is little information on how maturation, trafficking, and positioning of this subset of memory cells within specialized niches of the lung influence their ability to initiate a protective recall response to respiratory pathogens. This led us to investigate whether tissue-specific programs might exist at the cellular level, where different memory cell subsets specialize to elicit protective pathogen-specific recall responses.

RESULTS AND DISCUSSION

Phenotypic heterogeneity of memory CD8 T cells generated by intranasal VACV-WR infection

The presence of memory CD8 T cells in the lung has been associated with increased protection against respiratory virus infections (Kohlmeier and Woodland, 2009); however, it is unclear whether in situ immunity is caused by effector (CD27^{lo})- or central (CD27^{hi})-like memory cells trafficking to or resident in the lung tissue and airways. VACV is a good

Correspondence to Shahram Salek-Ardakani: ssalek@ufl.edu

Abbreviations used: 1°, primary; 2°, secondary; BALF, bronchoalveolar lavage fluid; IF, immunofluorescence; NT, no transfer; NYCBOH, New York City Board of Health; p.i., post-infection; Tcm-l, central-like T cell; Tem-l, effector-like T cell; VACV, vaccinia virus; WR, Western Reserve strain.

The Rockefeller University Press $30.00
J. Exp. Med. 2016 Vol. 213 No. 13 2897–2911
https://doi.org/10.1084/jem.20160167

model pathogen for studying the mechanisms by which different memory subpopulations control and eliminate highly pathogenic respiratory viruses. In mice, i.n. infection with the mouse-adapted VACV Western Reserve strain (VACV-WR) causes striking local and systemic changes that, in many respects, mimic human smallpox infection (Chapman et al., 2010). Initial VACV replication occurs in bronchiolar and alveolar epithelial cells, followed by a transient viremia that disseminates the virus throughout the host (Chapman et al., 2010). A lethal respiratory infection with VACV-WR leads to extensive lung pathology, peribronchial and perivascular inflammation, alveoli destruction, hemorrhage, rapid weight loss, and eventual death by day 8 (Chapman et al., 2010; Goulding et al., 2012).

Our previous studies have shown that heterogeneous populations of VACV-WR reactive memory CD8 cells play a vital role in restricting lung pathology and virus dissemination to visceral tissues, and are necessary for complete clearance of virus and protection from death (Salek-Ardakani et al., 2008, 2011b,c). However, as the relative contribution of different memory cell subsets was not directly examined, particularly regarding the $CD27^{hi}$ and $CD27^{lo}$ subset demarcation, we were interested in determining whether control of acute respiratory VACV-WR infection correlated with the presence and/or recruitment of these subsets to the site of infection.

First, we asked whether $CD27^{hi}$ and $CD27^{lo}$ memory cell subsets were established in the lung and lymphoid tissues after recovery from a respiratory infection with VACV-WR. Cohorts of naive WT C57BL/6 mice were infected i.n. with sublethal inoculum of VACV-WR (1.25×10^4 PFU), and the kinetics of effector and memory CD8 T cell recruitment to the lung and spleen were determined by tracking the immunodominant $B8R_{20–27}/k^b$-reactive population (Tscharke et al., 2005). Consistent with published data (Hikono et al., 2007), respiratory VACV-WR infection resulted in the generation of virus-specific $CD27^{hi}$ and $CD27^{lo}$ cells in both the lung and spleen (Fig. S1, A and B), with lung memory cells exhibiting a higher proportion of $CD27^{lo}$ cells (Fig. S1 B). A time-course analysis showed that after the contraction phase of the primary immune response the frequency of $CD27^{hi}$ and $CD27^{lo}$ memory cells in the spleen remained relatively stable for at least 2 yr (Fig. S1 C), whereas they strongly declined in the lung (Fig. S1 D). These data confirmed that the phenotype, subset composition, and persistence of the primary (1°) memory pool elicited by respiratory VACV infection is comparable to that observed after Sendai virus (Hikono et al., 2007), influenza virus (Hikono et al., 2007), or systemic VACV infection (Olson et al., 2013).

Protective capacity of $CD27^{hi}$ and $CD27^{lo}$ memory subsets against lethal infection

To investigate the relative importance of $CD27^{hi}$ and $CD27^{lo}$ cells to recall responses in the lung, we compared their capacity to protect against a lethal respiratory challenge with VACV-WR in an adoptive transfer model. To generate 1° memory T cells, cohorts of B6.SJL ($CD45.1^+$) donor mice were infected i.n. with a sublethal inoculum of VACV-WR (Fig. 1 A). 60 d later, $CD8^+CD44^{hi}$ cells from the spleen were FACS sorted into $CD27^{hi}$ and $CD27^{lo}$ subsets, normalized to ∼30,000 $B8R_{20–27}/k^b$ tetramer$^+$ cells, and injected i.v. into $CD45.2^+$ congenically marked naive C57BL/6 recipients (Fig. 1 B). As a positive control, infected mice were bled at the same time, and VACV-immune serum was prepared and transferred i.p. into a separate group of naive mice. The following day, all groups were challenged i.n. with a lethal inoculum of VACV-WR (2×10^6 PFU) and monitored for signs of illness and survival (Fig. 1, C and D). As demonstrated previously (Salek-Ardakani et al., 2011a,b; Goulding et al., 2012), naive mice that did not receive any memory CD8 T cells exhibited rapid weight loss and death within 8 d, whereas 100% were protected by transfer of hyperimmune (anti-VACV IgG) serum (Fig. 1 D). Although splenic $CD27^{lo}$ Tem-l cells eliminated VACV after systemic viral challenge (Olson et al., 2013), the same cells were unable to mediate protection against a respiratory challenge, and all animals succumbed to the infection with kinetics similar to naive controls (Fig. 1 D). In striking contrast, all mice that received $CD27^{hi}$ Tcm-l cells survived the infection and exhibited only moderate (15–20%) loss of body weight (Fig. 1 C), closely mirroring the illness and recovery observed in control mice that received VACV-specific serum. These responses were paralleled by the virus titers detected in the lungs and ovaries, which were completely cleared in $CD27^{hi}$ recipient mice, but not in $CD27^{lo}$ recipients or naive controls (Fig. 1 E). These observations strongly suggest that the antiviral activity of $CD27^{hi}$ Tcm-l cells within the microenvironment of the lung is distinct from that of $CD27^{lo}$ Tem-l cells and support the idea that the route of infection and target tissue influence the use of distinct memory subsets.

$CD27^{hi}$ Tcm-l cells use IFN-γ to protect against the lethal effects of VACV-infection

Mice deficient for IFN-γ are highly susceptible to respiratory VACV-WR infection, and IFN-γ production, primarily by effector CD8 T cells (Goulding et al., 2014), is essential for host recovery from a primary infection (Goulding et al., 2014; Abboud et al., 2015). Therefore, our next set of experiments was designed to assess whether IFN-γ produced by the transferred $CD27^{hi}$ Tcm-l cells was responsible for the protection against secondary challenge. To generate IFN-$\gamma^{-/-}$ memory cells, we took advantage of the fact that IFN-$\gamma^{-/-}$ mice survive VACV-WR when infected by the i.p. route (Goulding et al., 2014), and that these mice maintain normal numbers of functional memory CD8 T cells in the spleen with unaltered immunodominance hierarchy (unpublished data). As before, $CD27^{hi}$ memory cells were FACS sorted from the spleen of VACV-WR–infected IFN-$\gamma^{-/-}$ mice or WT controls and adoptively transferred into naive WT recipients, followed by infection with a lethal inoculum of

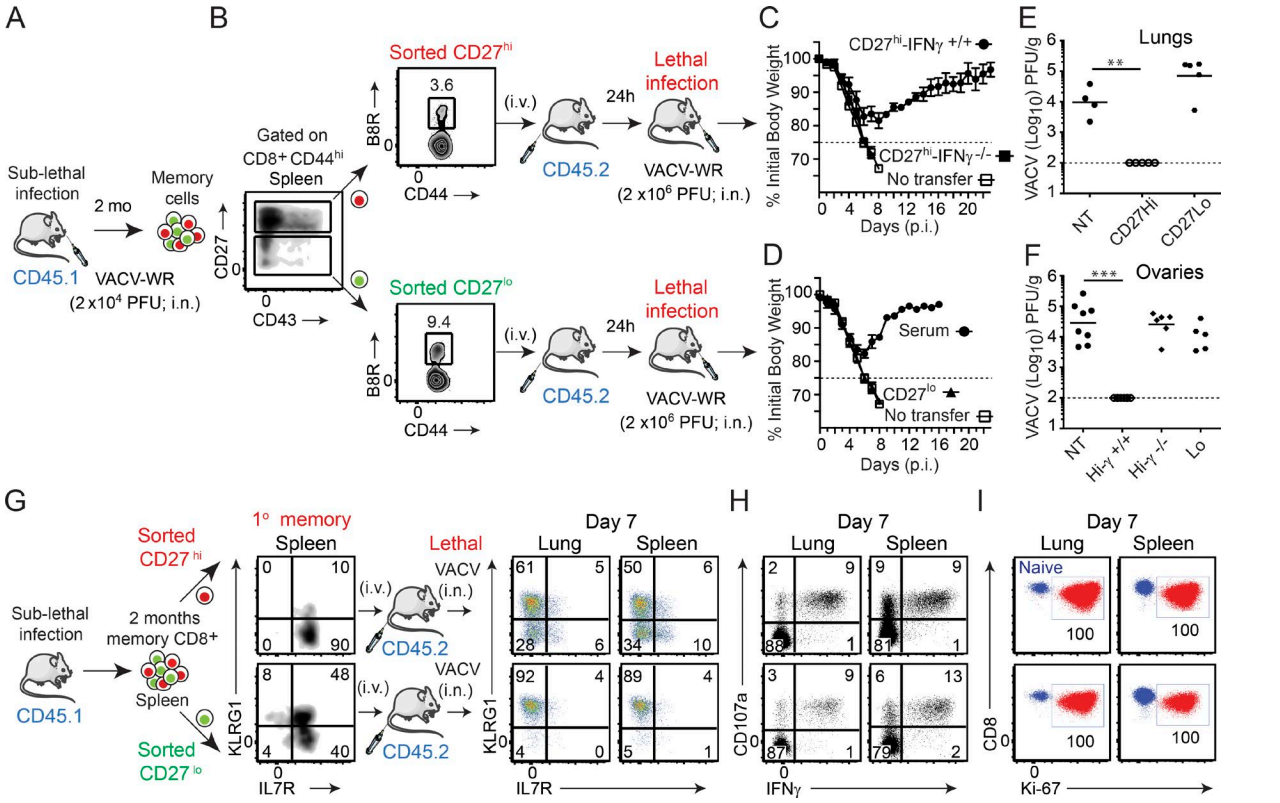

Figure 1. **CD27^{hi} memory CD8 T cells mediate optimal protection against lethal respiratory VACV-WR infection.** (A) Cohorts of WT donor mice (B6.SJL; CD45.1$^+$) were infected i.n. with VACV-WR (1.5×10^4 PFU/mouse). (B) Spleens were harvested 60 d later. Cells were enriched for CD8$^+$ cells on negative selection columns and sorted into CD8$^+$CD44^{hi}CD27^{hi} and CD8$^+$CD44^{hi}CD27^{lo} subsets by FACS. The sorted CD27^{hi} (C) and CD27^{lo} (D) cells were then adjusted such that the number of B8R$_{20-27}$/H-2K^b cells was equivalent (~30,000 tetramer$^+$ cells) and i.v. transferred into naive (CD45.2$^+$) recipient mice. (D) Some groups received 250 µl VACV-immune serum i.p. 1 d after transfer, recipient mice were infected i.n. with a lethal inoculum of VACV-WR (2×10^6 PFU). Naive mice that did not receive memory cells were used as controls (No transfer [NT]). Animals were weighed daily and euthanized if weight loss was >25% of initial body weight for two consecutive days. (C and D) Mean percent of initial body weight is shown. On day 7 after challenge lung (E) and ovaries (F) from individual mice that survived the infection were collected and virus titers were determined by plaque assay as described in Materials and methods. Dotted line indicates limit of detection for the plaque assay. Each symbol represents one mouse. (G–I) Mice that received CD8$^+$CD44^{hi} CD27^{hi} and CD27^{lo} memory T cells were analyzed on day 7 after infection. Lung and spleen mononuclear cells were harvested and stained for CD8α, CD44, KLRG1, IL-7Rα, CD45.1, B8R$_{20-27}$/K^b tetramer, intranuclear Ki-67, or stimulated with B8R peptide and subsequently stained for CD107a and intracellular IFN-γ. Representative plots for KLRG1/IL-7Rα (G), CD107a/IFN-γ (H), and Ki-67 (I) staining gated on CD8$^+$CD44^{hi}CD45.1$^+$B8R$_{20-27}$/K^b-tetramer$^+$ (G and I) and CD8$^+$CD44^{hi}CD45.1$^+$ (H) cells are shown. Numbers indicate percentages of positive cells within the gated population. Quadrant settings were based on controls, after gating on CD44^{lo} cells in the same host for phenotypic analysis or using infected cells that were not stimulated with peptide and uninfected cells stimulated with B8R peptide for functional analysis (not depicted). Data show one representative experiment of at least four with same results with at least four mice per experimental group. Error bars, SEM (C and D). **, $P < 0.01$; ***, $P < 0.001$ (two-tailed Student's *t* test).

VACV-WR. Adoptive transfer of i.p. generated WT CD27^{hi} memory cells afforded protection against death, which was comparable to that observed with i.n. generated cells (compare Fig. 1, E and F; and not depicted). In marked contrast, WT mice that received IFN-γ$^{-/-}$ CD27^{hi} memory cells failed to control the virus (Fig. 1 F), developed clinical symptoms similar to those observed in nontransferred naive controls, and all succumbed to the infection by day 8 (Fig. 1 C). This finding suggests that similar to primary effector CD8 T cells (Goulding et al., 2014), CD27^{hi} Tcm-l cells need to produce IFN-γ to protect against the lethal effects of secondary respiratory VACV-WR infection.

Functional characteristics of CD27^{hi} and CD27^{lo} CD8 T cell subpopulations

We sought to investigate the mechanism(s) underlying our observation that when compared with CD27^{lo} memory cells, CD27^{hi} memory cells were more protective against the lethal effects of respiratory VACV-WR infection. Our data pointed toward the release of IFN-γ as being a critical nonredundant component of CD27^{hi} memory cell–mediated protection; thus, we hypothesized that IFN-γ production by CD27^{lo} memory cells might be impacted by respiratory VACV-WR infection. At the time of peak response to VACV (7 d post-infection [p.i.]), analysis of B8R$_{20-27}$/k^b-tetramer$^+$ cells in both the lung

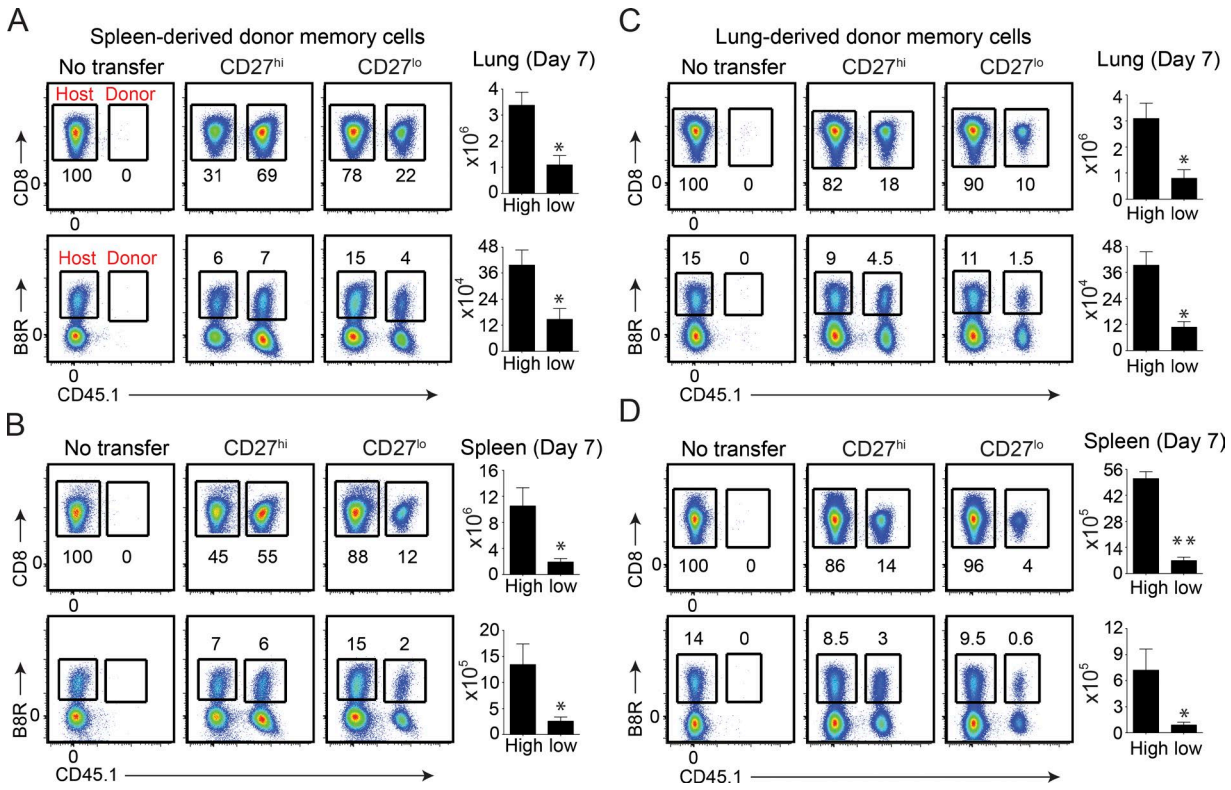

Figure 2. **CD27^{hi} memory CD8 T cells expand more than CD27^{lo} subset regardless of their tissue of origin.** Mice that received spleen- (A and B) or lung-derived (C and D) CD8$^+$CD44^{hi} CD27^{hi} and CD27^{lo} memory T cells were analyzed on day 7 after lethal infection. (top) Representative FACS plots showing total VACV-specific donor (CD45.1$^+$) cells as a percentage of CD8$^+$CD44^{hi} cells. (bottom) Representative FACS plots showing B8R$_{20-27}$/K^b tetramer$^+$ cells from the host (CD45.1$^-$) and each of the transferred (CD45.1$^+$) CD27^{hi} and CD27^{lo} populations as indicated. Naive mice that did not receive any memory cells (NT) were used as controls. Numbers indicate percentages of positive cells within the gated population. Total lung (A and C) and spleen (B and D) CD45.1$^+$ and B8R-reactive numbers presented as the mean ± SEM of three separate experiments with similar results containing three to four mice per group. *, $P < 0.05$; **, $P < 0.01$ (two-tailed Student's *t* test).

parenchyma and spleen showed that nearly all CD27^{lo} memory cells had up-regulated KLRG1 and down-regulated IL-7R (Fig. 1 G). This phenotype is indicative of a highly activated and differentiated CD8 T cells (Hikono et al., 2007). Most importantly, we found that CD27^{hi} and CD27^{lo} cells produced equivalent levels of IFN-γ, and both populations had degranulated similarly upon antigen stimulation (Fig. 1 H). Collectively, these results demonstrate that the failure of CD27^{lo} memory cells to control VACV was not due to either impaired priming or capacity to produce IFN-γ after trafficking to the lung tissue.

In situ accumulation of CD27^{hi} Tcm-l and CD27^{lo} Tem-l memory cells

We next asked whether the recall proliferative and in situ accumulation differed between CD27^{hi} and CD27^{lo} memory populations. To this end, CD8$^+$CD44^{hi}CD27^{hi} and CD8$^+$CD44^{hi}CD27^{lo} cells were isolated from the spleen 2 mo after sublethal infection and equal numbers of B8R$_{20-27}$/k^b-tetramer$^+$ cells were transferred separately into naive CD45.2 congenic recipients. In parallel experiments, we compared lung CD27^{hi} and CD27^{lo} memory cells from the same sets of mice. 1 d after transfer, recipient mice were infected i.n. with a lethal inoculum of VACV-WR and analyzed 8 d later. Our experimental design allowed comparison of primary (host; CD45.1$^-$) and secondary (donor; CD45.1$^+$) effector CD8 T cell responses in the absence of any preexisting VACV-specific antibodies. Moreover, transfer of total CD8$^+$CD44^{hi} cells allowed us to examine the recall response of both dominant and subdominant VACV-specific CD8 T cells. Interestingly, all of the adoptively transferred CD45.1$^+$CD27^{lo} and CD27^{hi} cells trafficking to or within the lung parenchyma (Fig. 1 I, left), spleen (Fig. 1 I, right), and draining lymph nodes (not depicted) stained positive for the cell cycle–specific protein Ki67, indicating that both dominant and subdominant populations had proliferated in response to VACV infection. However, analysis of both CD45.1$^+$ (total VACV-specific CD8 T cells; top) and B8R$_{20-27}$/k^b-tetramer$^+$ cells (bottom) revealed that CD27^{lo} cells weretwo to threefold less efficient at generating secondary (2°) effector T cells that could accumulate in the lung parenchyma (Fig. 2 A) and spleen (Fig. 2 B) compared with CD27^{hi} cells, in agreement with earlier findings in the Sendai virus (Hikono et al., 2007) and systemic VACV

(Olson et al., 2013) infection models. Notably, the same results were obtained when we used $CD27^{hi}$ Tcm-l and $CD27^{lo}$ Tem-l cells that were isolated from the lung (Fig. 2, C and D). Thus, regardless of their tissue of origin, $CD27^{hi}$ Tcm-l cells mediate stronger recall response than $CD27^{lo}$ Tem-l cells in terms their capacity to accumulate over time and protect.

$CD27^{hi}$ Tcm-l and $CD27^{lo}$ Tem-l cells localize to distinct anatomical niches within the lung

The data thus far implied that differential in situ accumulation of $CD27^{hi}$ and $CD27^{lo}$ memory cells, rather than their functionality, predicts protection against a lethal respiratory challenge with VACV-WR. In this regard, our previous studies (Salek-Ardakani et al., 2008, 2011b,c), which included direct adoptive transfer of memory CD8 T cells into the lungs, indicated that at least 10,000 memory cells needed to be present in the lung to allow the survival of the mice infected with a normally lethal inoculum of VACV-WR. This threshold was clearly achieved in mice that received $CD27^{lo}$ Tem-l cells. For example, on day 7 after infection, the total number of $B8R_{20–27}/k^b$-tetramer$^+$ and total virus-specific ($CD45.1^+$) effectors generated from $CD27^{lo}$ Tem-l donors in the lung was $\sim10^5$ and 10^6, respectively (Fig. 2 A). Thus, these data would argue against the absolute numbers of lung-infiltrating $CD27^{lo}$ cells as being the only contributing factor for their failure to control VACV. Indeed, when we transferred four times more $CD27^{lo}$ cells than $CD27^{hi}$ memory cells, which resulted in equal numbers of $B8R_{20–27}/k^b$-tetramer$^+$ $CD27^{lo}$ and $CD27^{hi}$ cells (unpublished data), $CD27^{lo}$ cells still failed to protect against lethal VACV challenge (unpublished data).

Immunofluorescence (IF) analysis of the distribution of $CD27^{hi}$ and $CD27^{lo}$ populations within the lung environment revealed striking and unexpected differences that help explain their differential contribution to viral clearance and recovery. In mice that received $CD27^{hi}$ memory cells, high numbers of $CD45.1^+$ donor 2° effector cells could be readily visualized egressing from the bronchial arteries that supply the bronchial regions, i.e., connective tissue around the arteries (Fig. 3 A), bronchi, and the lamina propria of the bronchioles (Fig. 3, A and B). Most significantly, $CD45.1^+CD27^{hi}$ donor cells were found in large numbers in direct contact with bronchiolar epithelium (Fig. 3 B, top and middle), where VACV infection and replication are commonly localized. Similar to $CD45.1^+CD27^{hi}$ donor cells, the $CD45.1^+CD27^{lo}$ 2° effectors were found in the connective tissue surrounding the arteries but showed a markedly different migration pattern through the bronchial regions. The majority of adoptively transferred $CD45.1^+CD27^{lo}$ donor cells localized in high numbers in the peribronchoarterial areas and in interalveolar septa but were mostly excluded from the bronchiolar epithelium (Fig. 3, C and D; and Fig. S2, A and B). To definitively show that $CD27^{lo}$ cells were localized to the interalveolar septa, we used CD34 to identify alveolar capillary endothelial cells and NG2 (nerve/glial antigen 2, Cspg4) to mark pericytes associated with the pre- and postcapillary vessels. (Fig. 3 E). As expected, we observed $CD45.1^+CD27^{lo}$ (donor) cells in the capillaries intimately associated with $CD34^+$ and in $NG2^+$ pulmonary capillaries (Fig. 3 E). Significantly, however, there were also abundant $CD45.1^+CD27^{lo}$ donor cells that were not associated with the aforementioned capillary markers (Fig. 3 E), indicating that $CD45.1^+CD27^{lo}$ 2° effectors are present within the vasculature as well as in the interalveolar septa. Next, we co-stained lung sections with NG2 and α-smooth muscle actin, which marks perivascular and peribronchiolar smooth muscle, as well as cells present discontinuously around the walls of the smallest venules. Importantly, and consistent with our other staining data, we could readily visualize $CD45.1^+CD27^{lo}$ cells outside of the vessels (Fig. 3 F). Together, these data provide compelling evidence that VACV-specific $CD27^{lo}$ cells are truly outside of vasculature. They further establish that $CD27^{lo}$ 2° effector memory cells occupy a spatially distinct niche of the lung in a region distant from the initial site of virus infection and replication.

Antiviral and inflammatory environment within the lungs of $CD27^{hi}$ Tcm-l– and $CD27^{lo}$ Tem-l–recipient mice

To understand the development of protective immune response to VACV and how homing preference of memory CD8 T cells within the lung is regulated, we compared the expression of 84 antiviral and inflammatory cytokine/chemokine genes from VACV-infected $CD27^{hi}$ and $CD27^{lo}$ recipient mice against naive mice, as well as VACV-infected WT mice that did not receive adoptive transfer of memory T cells. After disregarding unregulated, nondetectable gene products and presenting the relative levels of gene expression across all samples, we observed in adoptive transfer recipients (both $CD27^{lo}$ and $CD27^{hi}$) a dramatic (10–25 fold) increase in the expression of mRNA for chemokines associated with the receptors CCR5 (CCL3, CCL4, and CCL5) and CXCR3 (CXCL9 and CXCL10; Fig. 4, A and B), which have been implicated in coordinating the migration of virus-specific memory CD8 T cells to the sites of infection (Kohlmeier et al., 2011; Kastenmüller et al., 2013; Hickman et al., 2015). Surprisingly, however, we found little or no difference in the expression of these chemokines after virus challenge when comparing $CD27^{hi}$ and $CD27^{lo}$ recipient mice (Fig. 4 B). There were also no major differences (less than threefold) between $CD27^{hi}$ and $CD27^{lo}$ recipient mice in terms of their overall antiviral (Fig. 4 C) and cytokine/chemokine (Fig. 4 D) mRNA expression profiles after infection. In line with these observations, both the frequency and absolute numbers of antiviral innate immune cells, including NK cells, neutrophils, and inflammatory monocytes recovered from the lung, were comparable between the two groups of mice (unpublished data).

Differential expression of CXCR3 on VACV-specific $CD27^{hi}$ and $CD27^{lo}$ memory CD8 T cells

We next asked whether virus-specific $CD27^{hi}$ Tcm-l and $CD27^{lo}$ Tem-l cells generated after acute respiratory VACV infection differentially expressed the chemokine receptors

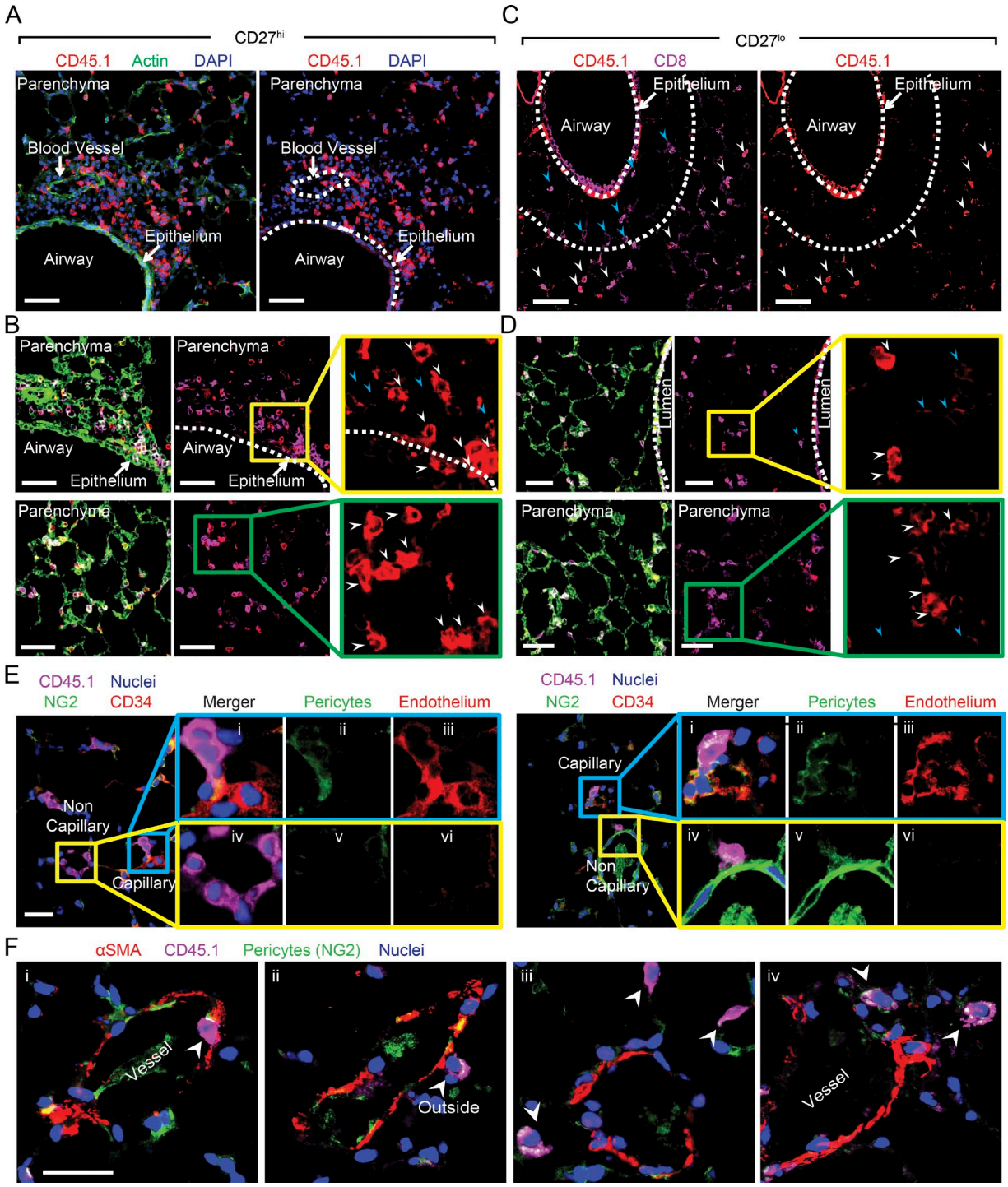

Figure 3. **Differential homing preference of CD27^{hi} and CD27^{lo} memory cells within the lung after lethal respiratory VACV-WR infection.** Mice that received CD8^{+}CD44^{hi} CD27^{hi} or CD27^{lo} memory T cells in Fig. 1 were analyzed on day 7 after infection. IF analysis of frozen lung sections from VACV-infected CD8^{+}CD44^{hi} CD27^{hi} (A and B) or CD8^{+}CD44^{hi} CD27^{lo} (C and D) recipient mice stained for CD45.1 (red) and CD8 (magenta). DAPI (blue) and ActinGreen (green) were used to visualize nuclei and lung morphology, respectively. Bars, 50 µm. Lung parenchyma, airway lumen, bronchial arteries are delineated by broken lines. The marked areas are shown in higher magnification to the right of each panel. CD45.1^{+} (red) donor cells are delineated with white arrows. Endogenous CD8 T cells could also be identified (magenta; blue arrows). (E) IF analysis of lung sections from aforementioned CD27^{lo} recipient mice stained with CD45.1 (magenta), NG2 (green), DAPI (blue), and CD34 (red) or (F) αSMA (red). Bars: (E and F) 10 µm. Results are representative of three experiments each with three mice per group.

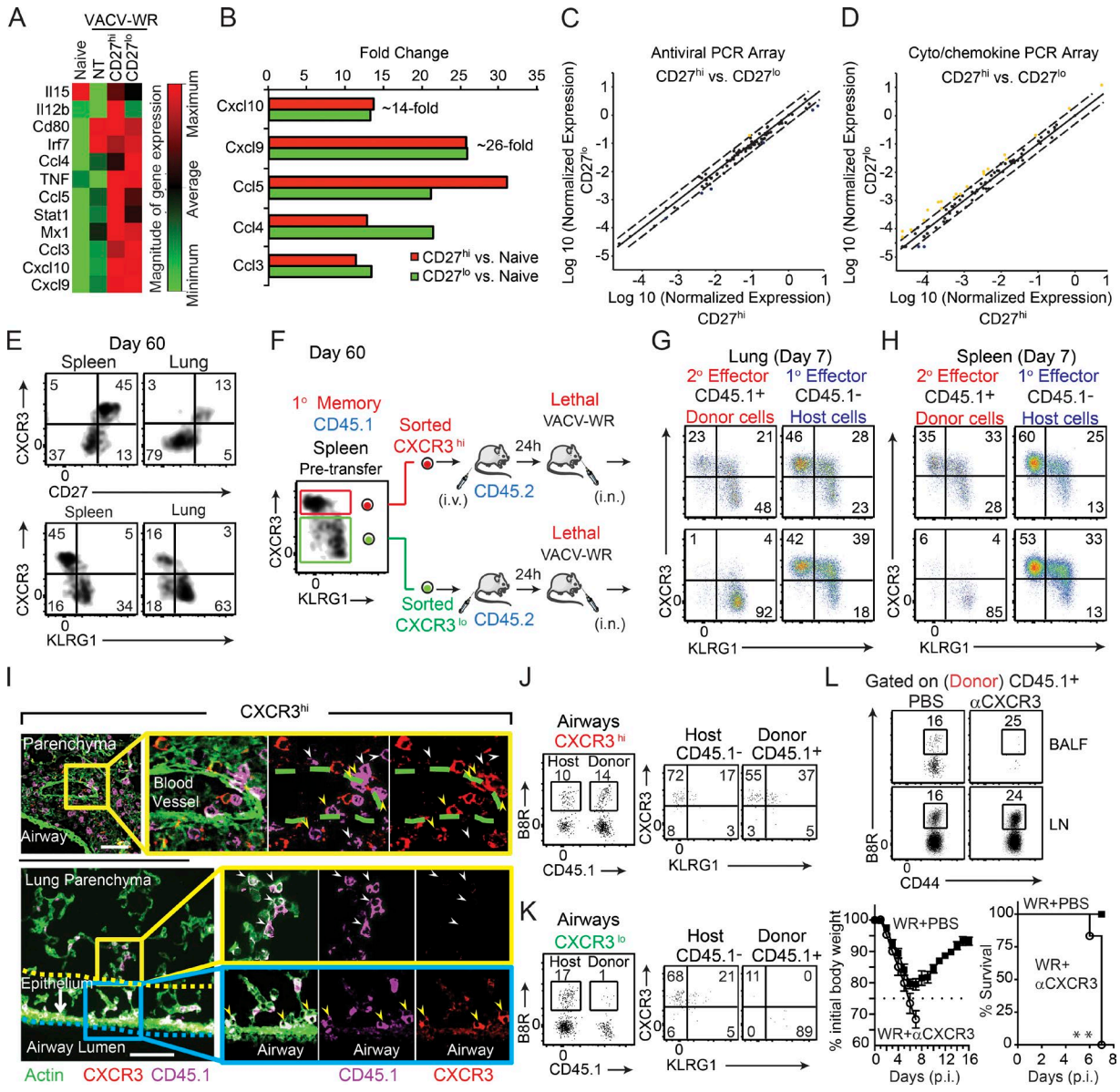

Figure 4. **CD27^{lo} effector cells are directly generated from CD27^{hi} memory populations, and CXCR3 expression determines their differential localization and protective value.** (A–D) Mice that received CD8^{+}CD44^{hi} CD27^{hi} and CD27^{lo} memory T cells in Fig. 1 were analyzed on day 7 after infection. One group of B6 mice did not receive any memory cell and used as a NT control. Total lung mRNA transcript levels of 84 antiviral and cytokine/chemokine genes were measured and presented as a heat map (A). Fold change in gene expression between CD27^{hi} recipients versus naive (B) CD27^{lo} recipients versus naive (B) CD27^{hi} versus CD27^{lo} recipient mice (C and D) is also presented. All array data are presented as the mean of gene expression level of four animals per group. (E) Representative FACS plots depict CD27/CXCR3 (top) and CXCR3/KLRG1 (bottom) expression profiles gated on B8R$_{20\text{-}27}$/K^{b} tetramer^{+} memory cells recovered from the spleen and lung 60 d after primary infection. Spleen memory cells were obtained as in Fig. 1 and sorted into CXCR3^{hi}KLRG^{lo} and CXCR3^{lo}KLRG^{hi} and i.v. injected into B6 (CD45.2^{+}) recipients that were lethally infected the next day with VACV-WR (F). Representative FACS plots depict CXCR3/KLRG1 profile of B8R$_{20\text{-}27}$/K^{b} tetramer-specific donor (secondary [2°] effectors) and host (primary [1°] effectors) cells in lungs (G) and spleens (H) 7 d after infection. (I) IFA of lung sections from CXCR3^{hi}-recipient mice were stained for CXCR3 (red), CD45.1 (magenta), and ActinGreen (green). Bars, 50 µm. The marked areas are shown in higher magnification to the right of each panel. Donor cells coexpressing CXCR3^{+} (red) and CD45.1^{+} (magenta) are indicated with yellow arrows, whereas donor CD45.1^{+} cells that down-regulated CXCR3 expression is delineated with white arrows. Endogenous cells could also be identified as only expressing CXCR3 (red only). Donor cells in close proximity to the airways epithelium are double positive. Bronchoalveolar lavage fluid from CXCR3^{hi} (J) and CXCR3^{lo} (K) recipient mice was harvested and stained for CD8α, CD44, KLRG1, CXCR3, CD45.1, and B8R$_{20\text{-}27}$/K^{b} tetramer. (left) Representative FACS plots showing B8R$_{20\text{-}27}$/K^{b} tetramer^{+} cells from the host (CD45.1^{-}) and each of the transferred (CD45.1^{+}) CXCR3^{hi} (J) and CXCR3^{lo} (K) populations as indicated. (right) Representative FACS plots for CXCR3/KLRG1 staining gated on CD8^{+}CD44^{hi}B8R$_{20\text{-}27}$/K^{b}-tetramer^{+} are shown. Numbers indicate percentages of positive cells within the gated population. (L) 30,000 B8R-tetramer^{+} CD8^{+}CD44^{hi}CXCR3^{hi} cells were i.v. transferred into naive (CD45.2^{+})

CXCR3 and CCR5. At steady state, <5% of naive ($CD44^{lo}$) T cells in the spleen express CXCR3, and all are negative for CCR5 (unpublished data). After primary infection, all $B8R_{20–27}/k^b$-tetramer$^+$ 1° effector cells in the spleen and lung up-regulated cell surface expression of CXCR3, whereas only a small fraction (<10%) expressed CCR5 (unpublished data). On day 60 after infection, a time point when memory cells were isolated for adoptive transfer experiments, the vast majority (>90%) of $CD27^{hi}$ $B8R_{20–27}/k^b$-tetramer$^+$ memory cells recovered from the spleen and lung had retained high surface expression of CXCR3 (Fig. 4 E, top), but were negative for expression of KLRG1 (Fig. 4 E, bottom) and CCR5 (not depicted). In striking contrast, very few (<5%) $CD27^{lo}$ $B8R_{20–27}/k^b$-tetramer$^+$ memory cells expressed CXCR3 in all sites sampled (Fig. 4 E, top). These findings are consistent with the hypothesis that differential expression of CXCR3 on $CD27^{hi}$ and $CD27^{lo}$ memory cells, rather than chemokine expression within the lung microenvironment, might be linked to their ability to home to airway epithelium and lumen.

$CD27^{lo}CXCR3^{lo}$ 2° effector cells are directly generated from $CD27^{hi}CXCR3^{hi}$ memory populations

To address the role of CXCR3 in homing preference of memory cells more directly, we adoptively transferred equal numbers of FACS-sorted $CD45.1^+CXCR3^{hi}$ ($CD27^{hi}KLRG1^{lo}$) and $CD45.1^+CXCR3^{lo}$ ($CD27^{lo}KLRG1^{hi}$) cells into naive WT recipients 1 d before lethal challenge (as illustrated in Fig. 4 F). At 7 d, when the adoptively transferred $CD45.1^+CXCR3^{lo}$ donor Tem-l cells were reanalyzed for the expression of CXCR3, KLRG1, and CD27, all cells maintained their original $CXCR3^{lo}$, $CD27^{lo}$, and $KLRG1^{hi}$ phenotype, regardless of whether they were isolated from the lung tissue (Fig. 4 G, bottom left) or spleen (Fig. 4 H, bottom left), whereas the majority of host ($CD45.1^-$) 1° effector cells were $CXCR3^{hi}$ (Fig. 4, G and H, bottom right). Intriguingly, when KLRG1 and CXCR3 were reanalyzed on the progeny of $CD45.1^+CXCR3^{hi}$ Tcm-l donor cells, three major subsets could be identified in the lung parenchyma: a minor population that maintained their original $KLRG1^{lo}CXCR3^{hi}$ phenotype (Fig. 4 G, top left quadrants); an intermediate population defined as $KLRG1^{hi}CXCR3^{hi}$ (Fig. 4 G, top right quadrants); and a terminally differentiated $KLRG1^{hi}$ population that exhibited a $CXCR3^{lo}$ phenotype (Fig. 4 G, bottom right quadrants). At the peak of the response to VACV, the terminally differentiated $KLRG1^{hi}CXCR3^{lo}$ population comprised 50–60% of total lung-resident 2° effector cells, which was substantially higher fraction than was found in the spleen (compare Fig. 4, G and H, top left). Notably, all three effector populations had proliferated and exhibited hallmarks of activated cells, including up-regulation of CD43 (unpublished data), as well as down-regulation of IL-7R (unpublished data). Comparison of CXCR3 expression on 2° (donor) versus 1° (endogenous) $B8R_{20–27}/k^b$-tetramer$^+$ effector populations in the same host revealed a significant shift from $CXCR3^{hi}$ to $CXCR3^{lo}$ phenotype in 2° effectors in all sites sampled, but particularly among the cells infiltrating the lung tissue. Together, these data indicate that $CD27^{lo}CXCR3^{lo}$ 2° effector cells are directly generated from $CD27^{hi}CXCR3^{hi}$ Tcm-l populations that have undergone further rounds of differentiation upon secondary antigen encounter.

The finding that a significant proportion of $CD27^{hi}$ $CXCR3^{hi}$ memory cells become $CD27^{lo}CXCR3^{lo}$ 2° effectors offered us the opportunity to explore their anatomical localization in the same host. At 7 d after VACV-WR infection, high numbers of $CD45.1^+CXCR3^{hi}$ donor 2° effector cells (Fig. 4 I; magenta [CD45.1], red stain [CXCR3]; double positive cells indicated by yellow arrows) could be visualized egressing from the bronchial arteries (Fig. 4 I, top) and in direct contact with airway epithelial cells (Fig. 4 I, bottom, yellow arrows). Notably, only $CD45.1^+CXCR3^+$, and not newly generated $CD45.1^+CXCR3^{lo}$, donor-derived $B8R_{20–27}/k^b$-tetramer$^+$ effector cells were recovered from the bronchoalveolar lavage fluid (BALF; Fig. 4 J), suggesting that CXCR3 plays an important role in recruitment of memory CD8 T cells to the lung airways during respiratory VACV infection. In line, newly generated $CD45.1^+CXCR3^{lo}$ 2° effectors were found in the connective tissue surrounding the arteries (Fig. 4 I, top, white arrows), but the majority of the cells showed reduced trafficking to the bronchiolar epithelium (Fig. 4 I, bottom, white arrows). Consistent with this pattern of migration, adoptively transferred $CD45.1^+CXCR3^{lo}$ ($CD27^{lo}$) donor cells localized in high numbers in interalveolar septa but were mostly excluded from the bronchiolar epithelium (Fig. S2 C). Again, this distribution was supported by flow cytometric observations in which very few $CD45.1^+CXCR3^{lo}$ donor 2° effectors were recovered from the BALF, whereas host-derived $CD45.1^-CXCR3^{hi}$ 1° effector CD8 T cells were readily visible in the same samples (Fig. 4 K).

To assess whether CXCR3 was responsible for the migration of $CD27^{hi}$ donor memory T cells to the airways after VACV infection, we performed several blocking experiments. Accordingly, $CD27^{hi}CXCR3^{hi}$ recipients were injected i.p. on days 1, 3, and 5 with a blocking mAb to CXCR3 (clone CXCR3-173) or PBS as control and the influx of donor cells to the airways was assessed on day 7 after infection. As expected, high numbers of donor cells were recovered from

recipient mice that were infected 1 d later with a lethal inoculum of VACV-WR. Infected mice were treated i.p. with PBS or mAb against CXCR3 on days 1, 3, and 5. Animals were analyzed on day 7. (top) Representative FACS plots showing $B8R_{20-27}/K^b$ tetramer$^+$ cells gated on the transferred $CD45.1^+$ cells. (bottom) Animals were weighed daily and euthanized if weight loss was >25% of initial body weight for two consecutive days. Mean percent of initial body weight is shown. Data are from one representative experiment of two with at least three mice per group (A–D and L) or at least three experiments with three and four mice per group (E–J). **, $P < 0.01$ (two-tailed Student's *t* test or Mantel-Cox test used in L).

in the BALF of control-treated $CD27^{hi}CXCR3^{hi}$ recipients, whereas neutralization of CXCR3 almost completely ablated their ability to traffic to the airways and protect against the lethal effects of infection (Fig. 4 L), reproducing the migratory and protective phenotype of $CD27^{lo}CXCR3^{lo}$ cells. Most significantly, systemic neutralization of CXCR3 had little or no effect on the frequency of total ($CD45.1^+$) and $B8R_{20–27}/k^b$-tetramer$^+$ 2° effector cells in the lung draining LNs (Fig. 4 L), demonstrating that impaired T cell migration to the airways is not caused by depletion of $CXCR3^+$ CD8 T cells. We also measured innate immune recruitment to the lungs and found that accumulation of NK cells, inflammatory monocytes, and neutrophils were not impacted by anti-CXCR3 mAb treatment (unpublished data). Collectively, these results provide evidence that donor $CD8^+$ T cell recruitment to the airways is primarily dependent on CXCR3 receptor–ligand interactions.

To formally test the relationship between localization of $CD27^{lo}CXCR3^{lo}$ and their protective function in the lung, we transferred $CD27^{lo}CXCR3^{lo}$ memory cells directly into the airways of naive recipients by intratracheal (i.t.) injection and subsequently challenged them i.n. with a lethal inoculum of VACV-WR. As a control, we i.t. injected the same number of $CD27^{hi}CXCR3^{hi}$ cells into parallel cohorts of mice (Fig. S2 D). As expected, mice that did not receive memory cells succumbed to the infection. In contrast, all of the mice were protected by direct airway transfer of $CD27^{hi}CXCR3^{hi}$ memory cells (Fig. S2 D). Remarkably, mice that received $CD27^{lo}CXCR3^{lo}$ memory cells were also protected and all recovered from the lethal infection, albeit with delayed kinetics compared with $CD27^{hi}CXCR3^{hi}$ cells (Fig. S2 D). Thus, $CD27^{lo}CXCR3^{lo}$ memory CD8 cells are fully functional and can protect against a highly lethal respiratory virus infection if localized to the initial sites of viral replication.

$CD27^{lo}CXCR3^{lo}$ 2° effector cells develop after entering the lung microenvironment

The appearance of $KLRG1^{hi}CXCR3^{lo}$ Tem-l cells in the infected lungs at the peak of the response to VACV suggested one of two possibilities: either activated T cells spontaneously began to down-regulate CXCR3 as the immune response progressed, or alternatively, they received additional tissue-specific signals in the new lung microenvironment after initial priming in the draining LNs. To distinguish between these two possibilities, we analyzed the kinetics of KLRG1 and CXCR3 expression on total ($CD45.1^+$) virus-specific (Fig. 5 A) and $B8R_{20–27}/k^b$-tetramer$^+$ (unpublished data) $CXCR3^{hi}$ donor cells isolated from different organs. Starting at 5 d, the $CXCR3^{hi}$ Tcm-l donor cells underwent extensive expansion (Fig. 5 A, top), and the vast majority (~60–80%) up-regulated KLRG1 expression, regardless of whether the cells were recovered from the lung tissue (Fig. 5 A, bottom left), draining lymph nodes, blood, or spleen (unpublished data). What is most noticeable is that, at this early time point, very few $KLRG1^+$ donor cells in the lung were $CXCR3^{lo}$ (Fig. 5 A). CXCR3 expression began to decrease on a significant fraction (40–50%) of virus-specific $KLRG1^+$ cells in the lung between days 5 and 7 p.i. (Fig. 5 A). Most significantly, a similar trend was not apparent for $KLRG1^+$ donor cells recovered from the draining LNs at the same time point (Fig. 5 B). Moreover, very few $KLRG1^+$ donor cells became $CXCR3^{lo}$ in the blood and spleen (Fig. 5 B). Together, these data provide compelling evidence that after leaving the draining LNs and migrating to the infected lung, a subset of $KLRG1^{hi}CXCR3^{hi}$ Tcm-l cells receive secondary environmental cues that instructs them to complete a full program of differentiation. This ultimately results in loss of CXCR3 expression and subsequent migration arrest and clustering around the vessels and interalveolar septa.

$CD27^{lo}CXCR3^{lo}$ 2° effector cells develop in response to high antigen load and viral virulence mechanisms

The significance of generating $CD27^{lo}CXCR3^{lo}$ Tem-l cells in the lung after respiratory VACV infection is not clear, though it may be related to host fitness. Indeed, VACV has the capacity to infect multiple innate immune cells, including monocytes and dendritic cells that have infiltrated or are in close proximity to the infectious foci and thereby facilitate rapid viral dissemination throughout the host. Interestingly, after infection with certain strains of Sendai and influenza viruses that only replicate locally, $CD27^{hi}$ Tcm-l cells did not down-regulate CXCR3 upon entering the lung parenchyma (Hikono et al., 2007). We speculated that differential anatomical distribution of $CD27^{hi}CXCR3^{hi}$ Tcm-l and $CD27^{lo}CXCR3^{lo}$ Tem-l populations provides layered immunological defense against highly virulent respiratory pathogens that have the capacity to spread rapidly beyond the initial site of infection. We considered the possibility that the inflammatory microenvironment created by less virulent viruses (or during low dose infections) may not provide the necessary co-signals that are needed to allow modulation of CXCR3 on lung-infiltrating T cells. Perhaps a certain threshold of antigen exposure and/or inflammation is required to allow the full program of differentiation to be initiated. To test this, we infected $CD27^{hi}CXCR3^{hi}$ Tcm-l recipient mice with 100- or 1,000-fold lower inoculum of VACV-WR and monitored the expression of KLRG1 and CXCR3 on donor cells (Fig. 5 C). As an additional test of our hypothesis, we used a replication-competent highly attenuated New York City Board of Health (NYCBOH) strain used as a smallpox vaccine in the United States (Dryvax; Wyeth). Whereas even a low dose of VACV-WR (10^4 or 10^3 PFU) was not controlled well, resulting in weight loss, 10^5 PFU NYCBOH was not pathogenic, and little to no weight loss was observed (Salek-Ardakani et al., 2011b; and unpublished data). At 7 d after infection, the frequency of total virus-specific and $B8R_{20–27}/k^b$-tetramer$^+$ donor cells in both the lung (Fig. 5, D and E) and secondary lymphoid organs (not depicted) was 2–30-fold greater in mice infected with 10^6 PFU WR than in those infected with 10^4 PFU, 10^3 PFU, or 10^5 PFU of NYCBOH, supporting our

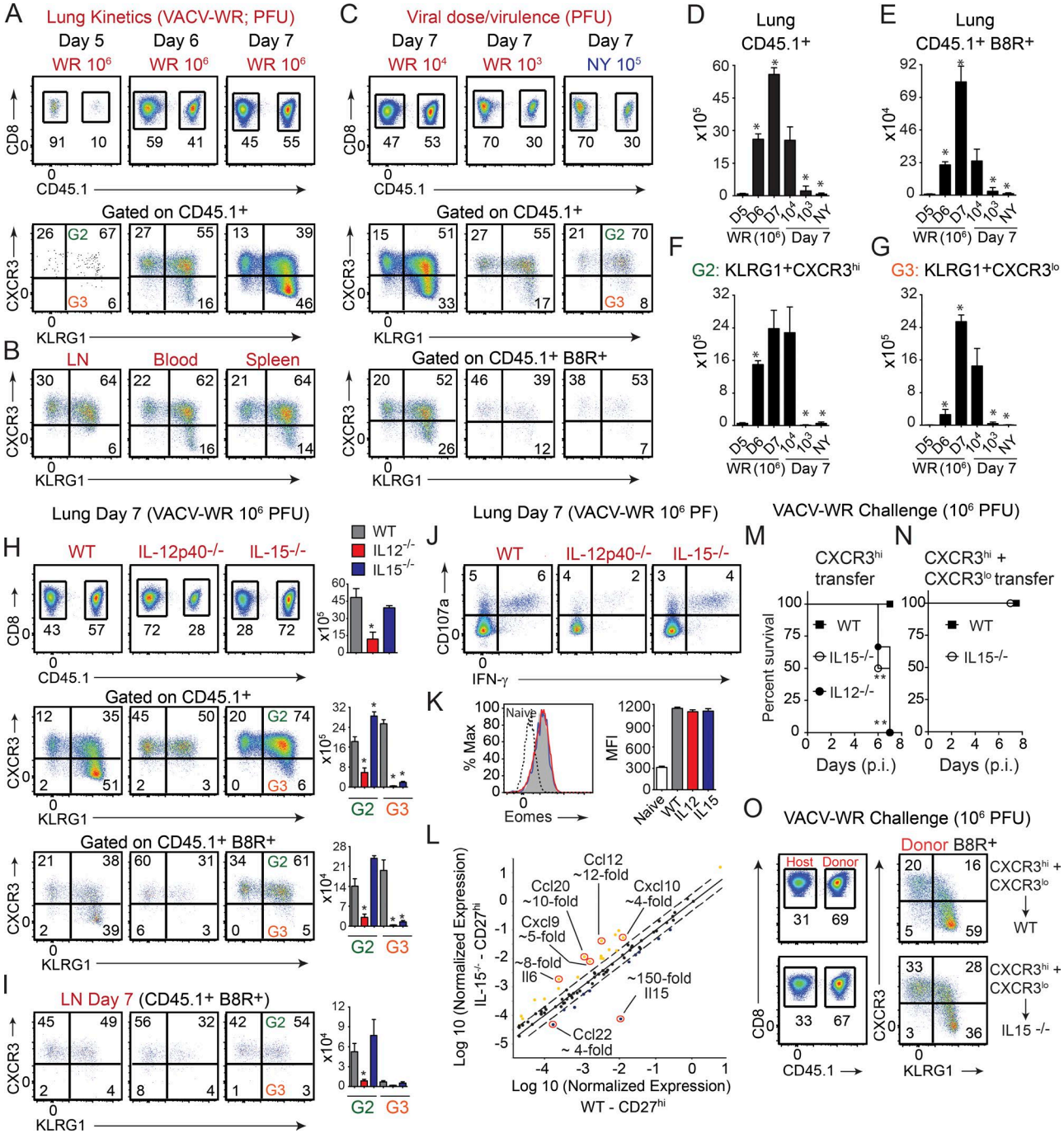

Figure 5. **Lung entry affects CXCR3 expression on central-like memory cells in a time- and virulence-dependent fashion and is cytokine driven.** Memory CD27^{hi}CXCR3^{hi} CD8 T cells were sorted from spleens of CD45.1+ SJL mice, i.v. transferred into naive (CD45.2^{+}) WT (A–G), IL-12p40$^{-/-}$ (H–K and N), and IL-15$^{-/-}$ (H–O) recipient mice that were i.n. infected next day with VACV-WR (10^6, 10^4, and 10^3 PFU) or attenuated VACV-NYCBOH (NY; 10^5 PFU) as indicated. Lung mononuclear cells were harvested on day 5 (A), 6 (A), and 7 (A–C and H–K) after infection and stained for CXCR3 and KLRG1 expression as in Fig. 4 F. (A, top) Representative plots of gated CD8^{+}CD44^{+} T cells staining for CD45.1 on the indicated days after infection; (bottom) Representative plots showing CXCR3 and KLRG1 expression gated on CD8^{+}CD44^{+}CD45.1^{+} donor cells. (B) Representative plots showing CXCR3 and KLRG1 expression gated on CD8^{+}CD44^{+}CD45.1^{+} donor cells recovered from the LNs, blood, and spleen. (C and H) Representative plots of gated CD8^{+}CD44^{+} T cells staining for CD45.1 (top) and CXCR3/ KLRG1 expression gated on total CD45.1^{+} (middle) and CD45.1^{+} B8R$_{20-27}$/K^{b}-tetramer^{+} (bottom) cells on day 7. Total numbers of CD45.1^{+} (D), CD45.1^{+} B8R$_{20-27}$/K^{b}-tetramer^{+} (E), CD45.1^{+}KLRG1^{+} (gate 2; F), and CD45.1^{+}KLRG1^{+}CXCR3^{lo} (gate 3; G) presented as the mean ± SEM of two separate experiments containing three mice per group. (I) Representative plots of gated CD8^{+}CD44^{+}CD45.1^{+} B8R$_{20-27}$/K^{b}-tetramer^{+} LN cells staining for CXCR3/ KLRG1 expression on day 7. Representative plots for CD107a/IFN-γ (J) and Eomesodermin (K) staining gated on CD8^{+}CD44^{hi}CD45.1^{+} cells recovered from the lung.

data that enhanced CD8 T cell expansion is related to the extent of viral load (Salek-Ardakani et al., 2011b). Analysis of CXCR3 expression showed that loss of cell surface expression on virus-specific donor cells was likely to be explained by altered inflammatory environment during secondary infection, as the extent of CXCR3 down-regulation directly correlated with the initial inoculum and virulence of VACV (Fig. 5 C, middle and bottom), again, mirroring the rate of virus clearance from the lung. Notably, lower frequencies (Fig. 5, F and G) of CXCR3^{lo} Tem-l cells after low dose/virulence infection was not caused by impaired activation of donor CD8 T cells in that KLRG1 (Fig. 5 C, middle and bottom) and CD43 (not depicted) were similarly elevated. Furthermore, the ability to produce IFN-γ and TNF on a per cell basis was almost identical between WR- and NYC BOH-infected groups over a wide range of viral doses (not depicted), suggesting that exposure to varying levels of viral antigen primarily affects the frequency and tissue-homing imprinting signals in the lung microenvironment, rather than the functional activity of individual cells.

Formation of CD27^{lo}CXCR3^{lo} 2° effector cells requires IL-12 and IL-15

The experiments described thus far indicated that a subset of recently recruited CD27^{hi}CXCR3^{hi} 2° Tcm-l cells within the lung may be exposed to a specific array of virus-induced inflammatory co-signals, and this may have stimulated their full program of differentiation to CD27^{lo}CXCR3^{lo} Tem-l cells. In this regard, it has been shown in other experimental systems that induction of IL-12 and IL-15 can, through both direct and indirect mechanisms, provide activation signals to effector and memory cells that alter their differentiation and homing patterns in vivo. To investigate a role for IL-12 and IL-15 signaling in the development of CD27^{lo}CXCR3^{lo} Tem-l cells, we transferred WT CD27^{hi}CXCR3^{hi} 1° memory cells into congenically marked IL-12– and IL-15–deficient recipient mice that we then infected with VACV-WR. At day 7 p.i., both percentages and numbers of total (CD45.1$^+$) virus-specific (Fig. 5 H, top) and B8R$_{20–27}$/k^b-tetramer$^+$ CXCR3^{hi} cells (not depicted) were strongly reduced in both lungs and draining LNs (Fig. 5 I) of IL-12$^{-/-}$ recipient mice when compared with cells in WT mice, and VACV-specific CD8 T cells that up-regulated KLRG1 (Fig. 5 H, middle and bottom), CD107a (Fig. 5 J), IFN-γ (Fig. 5 J), and T-bet (not depicted), were reduced by ∼50–70%. Concurrently, few if any CXCR3^{lo} donor cells were present in the lungs (Fig. 5 H) and LNs (Fig. 5 I) of the IL-12$^{-/-}$ recipient mice. In striking contrast, both the percentage and absolute numbers of VACV-specific CXCR3^{hi} donor cells were comparable between WT and IL-15$^{-/-}$ mice (Fig. 5, H and I). Most significantly, KLRG1 (Fig. 5, H and I), CD107a (Fig. 5 J), IFN-γ (Fig. 5 J), and Eomes (Fig. 5 K) were similarly elevated on VACV-reactive effector CD8 T cells in the lung of IL-15$^{-/-}$ mice as compared with WT mice, demonstrating that CD8 T cells were primed, able to migrate to the lung, and functional in the absence of IL-15. Despite this, only a small fraction (<10%) of activated KLRG1^{hi} cells fully differentiated to become CXCR3^{lo} effectors. Thus, IL-15 did not affect the size of the virus-specific effector population in the lung but reduced the expression of CXCR3.

One interpretation of these data could be that induction of Cxcl9 and Cxcl10 is impaired in IL-15$^{-/-}$ mice. To address this, the effect of IL-15 deficiency on the induction of total lung cytokine and chemokine mRNA levels was examined by gene pathway array. Interestingly, we found that Cxcl9 and Cxcl10, as well as several other chemokine genes, including Ccl12, Ccl2, Ccl20, Ccl4, Cxcl13, and Cxcl3, were all up-regulated in IL-15$^{-/-}$ recipient mice as compared with WT mice (Fig. 5 L). The elevated levels of Cxcl9 and Cxcl10 correlated with a marked influx of VACV-reactive donor cells within infected airway lumen (Fig. S3, A and B) and bronchiolar epithelium (Fig. S3 C). Comparable (<2.5-fold change) IFN-γ, IFN-α, IL-12, IL-18, IL-2, IL-23a, IL-7, and TNF mRNA levels were observed in the lungs of IL-15$^{-/-}$ and WT mice. As expected, no IL-15 mRNA expression was detected in lungs isolated from VACV-infected IL-15$^{-/-}$ mice. Collectively, these data suggest that early after infection, IL-12 predominantly dictates the frequency and initial differentiation of donor cells in the draining LNs, whereas IL-15 directs the secondary programming and homing preference of newly recruited T cells within the lung microenvironment.

CD27^{hi}CXCR3^{hi} memory cells fail to control lethal VACV infection in the absence of CD27^{lo}CXCR3^{lo} cells

Lastly, we addressed the significance of the spatial organization of Tem-l and Tcm-l memory cells in the lung. From our results in Fig. 1, it was clear that Tem-l CD27^{lo}CXCR3^{lo} cells in isolation could not orchestrate protective recall responses in the absence of the Tcm-l CD27^{hi}CXCR3^{hi} subset, consistent with the notion that for memory cells to completely clear VACV from the lungs, they must mobilize from the circulation to the infected airway lumen and bronchiolar epi-

(L) Total lung mRNA transcript levels of 84 cytokine and chemokine genes were measured from the same groups as in H and presented as scatter plot. Fold change in gene expression between CD27^{hi}CXCR3^{hi} WT and IL-15$^{-/-}$ recipients is presented. (M and N) CD27^{hi}CXCR3^{hi} (M) and total CD8$^+$CD44$^+$ CD8 T cells (containing a mixture of CD27^{hi}CXCR3^{hi} and CD27^{lo}CXCR3^{lo} cells; N) were sorted from spleens of CD45.1$^+$ SJL mice, i.v. transferred into naive (CD45.2$^+$) WT, IL-12p40$^{-/-}$, and IL-15$^{-/-}$-recipient mice that were i.n. infected the next day with a lethal inoculum of VACV-WR. Mean percent survival curves are shown. (O) Representative plots of gated CD8$^+$CD44$^+$ T cells staining for CD45.1 (left) and CXCR3/ KLRG1 expression (right) gated on CD45.1$^+$ B8R$_{20-27}$/K^b-tetramer$^+$ lung cells on day 7. Results are mean (n = 6–8 per group) from two experiments with similar results. *, $P < 0.05$; **, $P < 0.01$ (two-tailed Student's t test or Mantel-Cox test used in M and N).

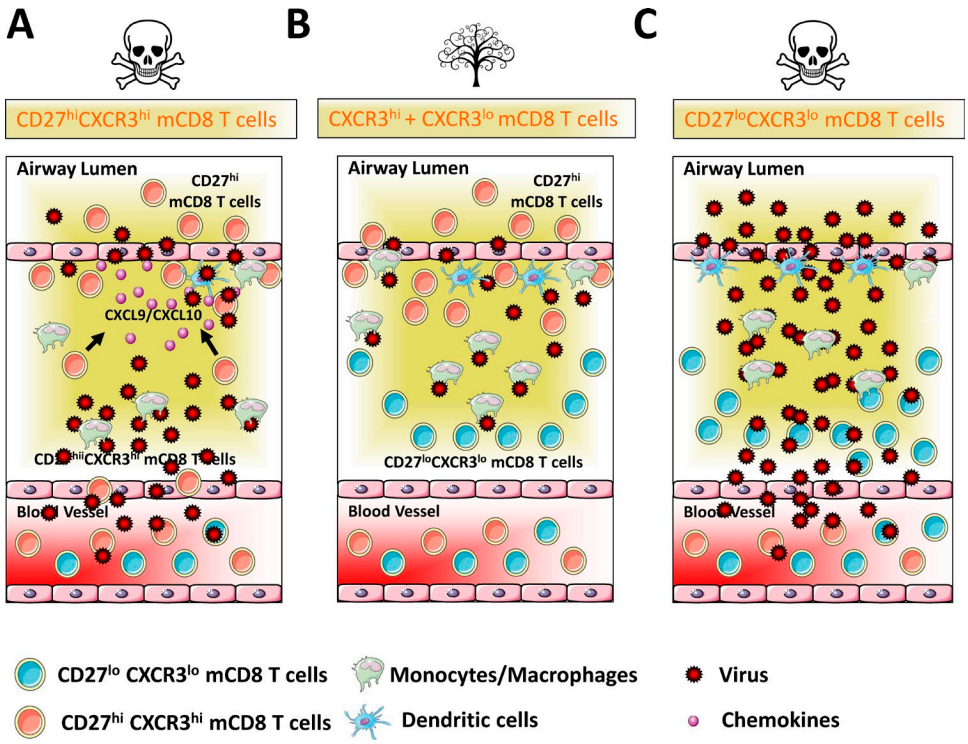

Figure 6. **Memory CD8 T cell subsets form tissue-specific layered defense to protect against lethal respiratory virus infection.** Airway epithelial cells serve as the primary location for virus-replication and spread after respiratory virus infection. (A) $CD27^{hi}CXCR3^{hi}$ memory CD8 T cells mobilize from the circulation into the lung parenchyma and airway epithelial foci cell and function as the first line of defense against pathogen exposure. (B) If mobile-infected cells successfully breach this first line of defense, the host possesses a second layer of protection, the $CD27^{lo}CXCR3^{lo}$ memory subsets, which are generated directly from $CD27^{hi}CXCR3^{hi}$ in situ in response to pathogen-specific inflammatory co-signals. Here, the immune system adapts its response to engage and kill infected cells to prevent systemic viral dissemination and eventual death. (C) $CD27^{lo}CXCR3^{lo}$ cannot mobilize to the epithelial foci and are eventually overwhelmed by the invading virus. The concept of layered immunity allows the adaptive immune system a certain level of plasticity to mount faster and stronger attacks each time the virus is encountered.

thelium foci. Because we found that a significant fraction of Tcm-l $CD27^{hi}CXCR3^{hi}$ cells become $CD27^{lo}CXCR3^{lo}$ after entering the lung microenvironment, it was unclear whether Tcm-l cells could recapitulate the full response required for protection in the absence of Tem-l subset or whether some degree of cooperation between these two subsets was necessary for immune protection.

To address this we examined IL-$15^{-/-}$ mice that contain Tcm-l $CD27^{hi}CXCR3^{hi}$ cells but lack Tem-l $CD27^{lo}CXCR3^{lo}$ 2° effectors. As before (Fig. 1), adoptive transfer of $CD27^{hi}CXCR3^{hi}$ into WT recipients afforded protection against death in this model (Fig. 5 M). Contrary to our expectations, IL-$15^{-/-}$ mice that received Tcm-l $CD27^{hi}CXCR3^{hi}$ cells failed to control the virus and all succumbed to infection by day 7 (Fig. 5 M). As expected, IL-$12^{-/-}$ recipient mice, which have reduced numbers of Tcm-l $CXCR3^{hi}$ and Tem-l $CXCR3^{lo}$ cells in the lung, were also found to be highly susceptible to infection, but exhibited more severe cachexia and immobility as compared with IL-$15^{-/-}$ mice (Fig. 5 M).

Consistent with the elevated chemokine mRNA levels observed in the lungs of VACV-infected IL-$15^{-/-}$ recipient mice (Fig. 5 L), we found that the recruitment and accumulation of neutrophils and inflammatory monocytes was enhanced in the absence of IL-15 (Fig. S3 D). As expected, no NK cells were observed in the lungs of VACV-infected IL-$15^{-/-}$ recipients (Fig. S3 D). We considered the possibility that lack of NK cells, rather than Tem-l $CXCR3^{lo}$ cells per se, might have been responsible for the enhanced susceptibility of IL-$15^{-/-}$ mice to lethal challenge. However, in our earlier study (Abboud et al., 2015), we had shown that absence of NK cells has little or no effect on the ability of mice to recover from a respiratory VACV-WR infection. Therefore, the interpretation that we favored is that the lack of protection observed in IL-$15^{-/-}$ recipients is caused by the absence of Tem-I cells in the infected lungs. Definitive proof for this came from adoptive co-transfer of $CXCR3^{hi}$ and $CXCR3^{lo}$ memory CD8 T cells into IL-$15^{-/-}$ mice (Fig. 5 N). In contrast to $CXCR3^{hi}$ single transfer group (Fig. 5 M), all IL-$15^{-/-}$ mice that received both $CXCR3^{hi}$ and $CXCR3^{lo}$ populations were protected from the lethal effects of infection (Fig. 5 N). The presence of VACV-specific $CXCR3^{lo}$ donor cells in the lungs of IL-$15^{-/-}$ mice confirmed that

CD8 T cells were primed and able to migrate to the site of infection in the absence of IL-15 (compare Fig. 5, H and O, third row). Together, these data provide compelling evidence that protective immunity provided by virus-specific memory CD8 T cells requires coordinated action of Tem-l and Tcm-l subsets. In this study, we propose a novel model for respiratory immunity (Fig. 6) in which $CD27^{hi}CXCR3^{hi}$ Tcm-l memory cells efficiently localize to the epithelial foci and are able to control virus replication at the initial sites of pathogen exposure, but they are likely unable to eliminate mobile virus-infected immune cells. Thus, we propose that $CD27^{lo}CXCR3^{lo}$ 2° Tem-l cells, localized in high numbers in the peribronchoarterial areas and in interalveolar septa, form a second layer of defense, which can engage and kill infected cells that escape initial clearance to prevent systemic viral dissemination and eventual death.

These findings are noteworthy, as much of what is known regarding the relative contribution of memory populations during recall responses to respiratory viruses is related to their proliferative potential rather than their protective capacity (Ely et al., 2003; Roberts and Woodland, 2004; Roberts et al., 2005; Hikono et al., 2007). Although $CD27^{hi}$ central-like memory cells indeed exhibit greater capacity for recall proliferative responses, effector-like cells have been claimed to provide superior protection, primarily by engaging pathogens at the initial sites of exposure. Indeed, as previously mentioned, the protective capacity of $CD27^{hi}$ Tcm-l and $CD27^{lo}$ Tem-l subpopulations was observed within the spleen after systemic infection with VACV (Olson et al., 2013). Here, $CD27^{lo}$ but not $CD27^{hi}$ cells were found to preferentially localize in the red pulp (the primary points of contact between CD8 T cells and blood-borne pathogens) and were more effective at preventing VACV replication than $CD27^{hi}$ cells. Our finding that $CD27^{lo}$ effector-like memory cells tend to congregate in clusters far from airway epithelium, together with their apparent failure to clear virus from the lung tissue, challenges this paradigm. Instead, it appears that, in the respiratory tract, $CD27^{hi}$ Tcm-l cells function as frontline defenses by rapidly mobilizing to the initial sites of viral entry and infectious foci. Together, these studies highlight the complexities of antiviral immunity and reinforce the idea that phenotypic and functional heterogeneity in the memory pool provides the host certain level of plasticity in terms of its capacity to combat pathogens encountered via different routes.

Our current study has important implications for vaccine design. Previous studies suggest that peripheral prime-boost regimens, to induce secondary and possibly tertiary effector-like memory CD8 T cells, are required for long-lasting immunity (Woodland, 2004; Butler et al., 2011; Nolz and Harty, 2011). Although this is likely true for elimination of blood-borne pathogens in certain lymphoid tissues, the predominance of $CD27^{lo}$ Tem-l cells in the memory pool that frequently occurs after repetitive antigen encounters will likely provide insufficient protection against respiratory pathogens. Thus, the challenge for the future will be to develop strategies that induce localization of pathogen-specific Tcm-l $CD27^{hi}$ CD8 memory cells within the lung epithelium and, at the same time, shift the balance of cell differentiation from a $CD27^{hi}$ to a $CD27^{lo}$ phenotype, allowing for layered immunological defense against highly virulent respiratory viruses.

MATERIALS AND METHODS

Mice

8–12-wk-old female C57BL/6 (CD45.2), B6.SJL-*Ptprc*^{a} *Pepc*^{b}/BoyJ (CD45.1/Ly5.1), and B6.129S7-*Ifng*^{tm1Ts}/J mice were either purchased from The Jackson Laboratory or bred and maintained at the University of Florida animal facility. All animal protocols were approved by the Institutional Animal Care and Use Committee (IACUC) of the University of Florida (Gainesville, FL; OLAW Assurance # A3377-01).

Virus and peptides

VACV-WR was purchased from the ATCC, grown in HeLa cells, and subsequently titered on VeroE6 cells as described previously (Salek-Ardakani et al., 2008). The VACV-WR peptide B8R (20–27; TSYKFESV; Tscharke et al., 2005; Moutaftsi et al., 2006) was purchased From A & A Labs. Major MHC/peptide tetramers containing the B8R peptide (20–27; TSYKFESV)/H-$2K^{b}$, conjugated to allophycocyanin (APC), were obtained from the National Institutes of Health Tetramer Core facility (Emory University, Atlanta, GA).

Flow cytometric and FACS analysis

Preparation of cells, extracellular/intracellular staining, data acquisition, and data analysis were performed as described previously (Salek-Ardakani et al., 2011b; Flynn et al., 2013; Goulding et al., 2014).

IF studies

At the indicated times VACV-infected lungs were inflated with 500 µl 50:50 OCT/PBS embedding solution and immediately snap frozen on dry ice. Frozen blocks were cut into 6-µm sections, fixed in acetone, blocked in a 5% BSA PBS solution for 1 h, and stained with DAPI (Invitrogen) and antibodies specific for CD45.1 (clone A20), CD8 (clone 53–6.7), CXCR3 (CXCR3-173), and actin Green 488 Ready Probes. Analysis of microscopy images was performed as previously described (Flynn et al., 2013; Goulding et al., 2014).

Statistical analysis

Tests were performed using Prism 5.0 software (GraphPad). Statistics were done using two-tailed, unpaired Student's *t* test with 95% confidence intervals unless otherwise indicated. Two-way ANOVA was used to determine differences in weight loss profiles and the Mantel-Cox test was used for survival analysis. Unless otherwise indicated, data represent the mean ± SEM; $P < 0.05$ considered statistically significant.

Online supplemental material

Fig. S1 shows the composition and kinetics of splenic and lung memory $CD8^+$ T cell subsets after sublethal respiratory VACV-WR infection. Fig. S2 shows the method of enumerating VACV-specific donor cells in the peribronchiolar regions of the lungs and the localization of $CD27^{lo}$ ($CXCR3^{lo}$) within the lungs at day 7 after lethal infection, as well as the weight loss curve obtained with the two CD8 memory subsets when provided directly in the airways followed by a lethal VACV infection. Fig. S3 shows the recruitment of $CD27^{hi}$ ($CXCR3^{hi}$) memory $CD8^+$ T cell subset to the airway lumen and epithelium in IL-$15^{-/-}$ mice as well as the lung innate immune response after lethal respiratory VACV infection.

ACKNOWLEDGMENTS

We thank the National Institutes of Health Tetramer Core Facility (contract HHSN272201300006C) for provision of MHC/peptide tetramer containing the B8R peptide (20–27; TSYKFESV)/H-$2K^b$, conjugated to APC.

This work was supported by National Institutes of Health grant AI087734 to S. Salek-Ardakani. V. Tahiliani was supported by National Institutes of Health grant T32 AR007603-15. P. Desai was supported through The American Association of Immunologists Careers in Immunology Fellowship Program.

The authors declare no competing financial interests.

Submitted: 2 February 2016
Revised: 9 June 2016
Accepted: 21 October 2016

REFERENCES

Abboud, G., V. Tahiliani, P. Desai, K. Varkoly, J. Driver, T.E. Hutchinson, and S. Salek-Ardakani. 2015. Natural killer cells and innate interferon gamma participate in the host defense against respiratory vaccinia virus infection. *J. Virol.* 90:129–141. http://dx.doi.org/10.1128/JVI.01894-15

Butler, N.S., J.C. Nolz, and J.T. Harty. 2011. Immunologic considerations for generating memory CD8 T cells through vaccination. *Cell. Microbiol.* 13:925–933. http://dx.doi.org/10.1111/j.1462-5822.2011.01594.x

Chapman, J.L., D.K. Nichols, M.J. Martinez, and J.W. Raymond. 2010. Animal models of orthopoxvirus infection. *Vet. Pathol.* 47:852–870. http://dx.doi.org/10.1177/0300985810378649

Ely, K.H., A.D. Roberts, and D.L. Woodland. 2003. Cutting edge: effector memory $CD8^+$ T cells in the lung airways retain the potential to mediate recall responses. *J. Immunol.* 171:3338–3342. http://dx.doi.org/10.4049/jimmunol.171.7.3338

Flynn, R., T. Hutchinson, K.M. Murphy, C.F. Ware, M. Croft, and S. Salek-Ardakani. 2013. CD8 T cell memory to a viral pathogen requires trans cosignaling between HVEM and BTLA. *PLoS One.* 8:e77991. http://dx.doi.org/10.1371/journal.pone.0077991

Goulding, J., R. Bogue, V. Tahiliani, M. Croft, and S. Salek-Ardakani. 2012. CD8 T cells are essential for recovery from a respiratory vaccinia virus infection. *J. Immunol.* 189:2432–2440. http://dx.doi.org/10.4049/jimmunol.1200799

Goulding, J., G. Abboud, V. Tahiliani, P. Desai, T.E. Hutchinson, and S. Salek-Ardakani. 2014. CD8 T cells use IFN-γ to protect against the lethal effects of a respiratory poxvirus infection. *J. Immunol.* 192:5415–5425. http://dx.doi.org/10.4049/jimmunol.1400256

Hickman, H.D., G.V. Reynoso, B.F. Ngudiankama, S.S. Cush, J. Gibbs, J.R. Bennink, and J.W. Yewdell. 2015. CXCR3 chemokine receptor enables local $CD8^+$ T cell migration for the destruction of virus-infected cells. *Immunity.* 42:524–537. http://dx.doi.org/10.1016/j.immuni.2015.02.009

Hikono, H., J.E. Kohlmeier, S. Takamura, S.T. Wittmer, A.D. Roberts, and D.L. Woodland. 2007. Activation phenotype, rather than central- or effector-memory phenotype, predicts the recall efficacy of memory $CD8^+$ T cells. *J. Exp. Med.* 204:1625–1636. http://dx.doi.org/10.1084/jem.20070322

Jameson, S.C., and D. Masopust. 2009. Diversity in T cell memory: an embarrassment of riches. *Immunity.* 31:859–871. http://dx.doi.org/10.1016/j.immuni.2009.11.007

Jung, Y.W., R.L. Rutishauser, N.S. Joshi, A.M. Haberman, and S.M. Kaech. 2010. Differential localization of effector and memory CD8 T cell subsets in lymphoid organs during acute viral infection. *J. Immunol.* 185:5315–5325. http://dx.doi.org/10.4049/jimmunol.1001948

Kastenmüller, W., M. Brandes, Z. Wang, J. Herz, J.G. Egen, and R.N. Germain. 2013. Peripheral prepositioning and local CXCL9 chemokine-mediated guidance orchestrate rapid memory CD8+ T cell responses in the lymph node. *Immunity.* 38:502–513. http://dx.doi.org/10.1016/j.immuni.2012.11.012

Kohlmeier, J.E., and D.L. Woodland. 2009. Immunity to respiratory viruses. *Annu. Rev. Immunol.* 27:61–82. http://dx.doi.org/10.1146/annurev.immunol.021908.132625

Kohlmeier, J.E., W.W. Reiley, G. Perona-Wright, M.L. Freeman, E.J. Yager, L.M. Connor, E.L. Brincks, T. Cookenham, A.D. Roberts, C.E. Burkum, et al. 2011. Inflammatory chemokine receptors regulate $CD8^+$ T cell contraction and memory generation following infection. *J. Exp. Med.* 208:1621–1634. http://dx.doi.org/10.1084/jem.20102110

Masopust, D., V. Vezys, A.L. Marzo, and L. Lefrançois. 2001. Preferential localization of effector memory cells in nonlymphoid tissue. *Science.* 291:2413–2417. http://dx.doi.org/10.1126/science.1058867

Moutaftsi, M., B. Peters, V. Pasquetto, D.C. Tscharke, J. Sidney, H.H. Bui, H. Grey, and A. Sette. 2006. A consensus epitope prediction approach identifies the breadth of murine $T(CD8^+)$-cell responses to vaccinia virus. *Nat. Biotechnol.* 24:817–819. http://dx.doi.org/10.1038/nbt1215

Nolz, J.C., and J.T. Harty. 2011. Strategies and implications for prime-boost vaccination to generate memory CD8 T cells. *Adv. Exp. Med. Biol.* 780:69–83. http://dx.doi.org/10.1007/978-1-4419-5632-3_7

Olson, J.A., C. McDonald-Hyman, S.C. Jameson, and S.E. Hamilton. 2013. Effector-like $CD8^+$ T cells in the memory population mediate potent protective immunity. *Immunity.* 38:1250–1260. http://dx.doi.org/10.1016/j.immuni.2013.05.009

Roberts, A.D., and D.L. Woodland. 2004. Cutting edge: effector memory $CD8^+$ T cells play a prominent role in recall responses to secondary viral infection in the lung. *J. Immunol.* 172:6533–6537. http://dx.doi.org/10.4049/jimmunol.172.11.6533

Roberts, A.D., K.H. Ely, and D.L. Woodland. 2005. Differential contributions of central and effector memory T cells to recall responses. *J. Exp. Med.* 202:123–133. http://dx.doi.org/10.1084/jem.20050137

Salek-Ardakani, S., M. Moutaftsi, S. Crotty, A. Sette, and M. Croft. 2008. OX40 drives protective vaccinia virus-specific CD8 T cells. *J. Immunol.* 181:7969–7976. http://dx.doi.org/10.4049/jimmunol.181.11.7969

Salek-Ardakani, S., Y.S. Choi, M. Rafii-El-Idrissi Benhnia, R. Flynn, R. Arens, S. Shoenberger, S. Crotty, M. Croft, and S. Salek-Ardakani. 2011a. B cell-specific expression of B7-2 is required for follicular Th cell function in response to vaccinia virus. *J. Immunol.* 186:5294–5303. http://dx.doi.org/10.4049/jimmunol.1100406

Salek-Ardakani, S., R. Flynn, R. Arens, H. Yagita, G.L. Smith, J. Borst, S.P. Schoenberger, and M. Croft. 2011b. The TNFR family members OX40 and CD27 link viral virulence to protective T cell vaccines in mice. *J. Clin. Invest.* 121:296–307. http://dx.doi.org/10.1172/JCI42056

Salek-Ardakani, S., M. Moutaftsi, A. Sette, and M. Croft. 2011c. Targeting OX40 promotes lung-resident memory CD8 T cell populations that protect against respiratory poxvirus infection. *J. Virol.* 85:9051–9059. http://dx.doi.org/10.1128/JVI.00619-11

Sallusto, F., D. Lenig, R. Förster, M. Lipp, and A. Lanzavecchia. 1999. Two subsets of memory T lymphocytes with distinct homing potentials and effector functions. *Nature.* 401:708–712. http://dx.doi.org/10.1038/44385

Sathaliyawala, T., M. Kubota, N. Yudanin, D. Turner, P. Camp, J.J. Thome, K.L. Bickham, H. Lerner, M. Goldstein, M. Sykes, et al. 2013. Distribution and compartmentalization of human circulating and tissue-resident memory T cell subsets. *Immunity.* 38:187–197. http://dx.doi.org/10.1016/j.immuni.2012.09.020

Thome, J.J., N. Yudanin, Y. Ohmura, M. Kubota, B. Grinshpun, T. Sathaliyawala, T. Kato, H. Lerner, Y. Shen, and D.L. Farber. 2014. Spatial map of human T cell compartmentalization and maintenance over decades of life. *Cell.* 159:814–828. http://dx.doi.org/10.1016/j.cell.2014.10.026

Tscharke, D.C., G. Karupiah, J. Zhou, T. Palmore, K.R. Irvine, S.M. Haeryfar, S. Williams, J. Sidney, A. Sette, J.R. Bennink, and J.W. Yewdell. 2005. Identification of poxvirus CD8+ T cell determinants to enable rational design and characterization of smallpox vaccines. *J. Exp. Med.* 201:95–104. http://dx.doi.org/10.1084/jem.20041912

Woodland, D.L. 2004. Jump-starting the immune system: prime-boosting comes of age. *Trends Immunol.* 25:98–104. http://dx.doi.org/10.1016/j.it.2003.11.009